# Ferroelectric annular domains in hexagonal manganites

J. Li,[1] H. X. Yang,[1] H. F. Tian,[1] S.-W. Cheong,[2] C. Ma,[1] S. Zhang,[3] Y. G. Zhao,[3] and J. Q. Li[1,*]

[1]*Beijing National Laboratory for Condensed Matter Physics, Institute of Physics, Chinese Academy of Sciences, Beijing 100190, China*
[2]*Rutgers Center for Emergent Materials and Department of Physics and Astronomy, Rutgers University, Piscataway, New Jersey 08854, USA*
[3]*Department of Physics and State Key Laboratory of Low-Dimensional Quantum Physics, Tsinghua University, Beijing 100084, China*

(Received 24 June 2012; revised manuscript received 17 October 2012; published 12 March 2013)

Experimental observations and theoretical simulations for the ferroelectric (FE) domains in multiferroic $R\mathrm{MnO_3}$ ($R$=Ho-Lu, Y, and Sc) demonstrate that annular domains can appear in the topological Kosterlitz-Thouless (KT) phase in coexistence with the "cloverleaf" vortices. Moreover, the annular domains often adopt the multilayered structures as indexed by the annular number. The double-layered FE domains, an energetically favored structure, are commonly found in $R\mathrm{MnO_3}$. Thermal annealing experiments directly show exchanges between large annular domains and cloverleaf vortices above the trimerization-structural transition temperature $T_c$. The temperature evolution of the FE domains has been analyzed by using the six-state clock model through Monte Carlo simulations. Based on careful *in situ* SEM observations, the dynamic properties of annular domains and interplay among domain walls have been briefly discussed.

DOI: 10.1103/PhysRevB.87.094106 PACS number(s): 77.80.Dj, 68.37.Og, 77.80.Fm

Multiferroic materials have received much attention because of their wide range of applications such as nonvolatile random-access memory, nanoscale sensors, photonic crystals, and biologically inspired nanostructures.[1–4] There are three well-known forms of the ferroic orders in correlation with spontaneous magnetization (ferromagnetism), electric polarization (ferroelectricity), and spontaneous strain (ferroelasticity), respectively. Ferroelectricity often accompanies ferroelastic strain, so ferroelectric (FE) domains tend to form in simple elongated configurations such as stripes.[5,6] On the other hand, it is also noted that the localized magnetic and FE domains have been also investigated in certain remarkable systems, e.g., magnetic bubbles have been observed in magnetic films under applied magnetic fields and used to build experimental devices that are of great interest in engineering practical electronic devices.[7–9] In this paper we will report on structural features and polarization configurations for the annular domains observed in hexagonal manganites. In addition, it is also demonstrated by using Monte Carlo simulations based on the six-state clock model that annular domains can appear in a large temperature range and often coexist with vortex domains in the Kosterlitz-Thouless (KT) ordered state.

Recent investigations of layered hexagonal $R\mathrm{MnO_3}$ ($R$=Ho-Lu, Y, and Sc) have revealed interesting FE domain structures and remarkable physical properties, such as "cloverleaf" vortex structures[10] and anisotropic conductivity at domain walls.[11] In order to clearly reveal the microstructural features of the ferroelectric domains at a high spatial resolution, we combined transmission electron microscopy (TEM), scanning electron microscopy (SEM), and piezoresponse force microscopy (PFM) for our analysis. In particular, we have demonstrated that scanning secondary-electron microscopy with operating voltage ($V_0$) less than 1 kV could be a powerful technique to directly reveal the FE domain/wall structures.[12] In addition, we also performed Monte Carlo simulations on the two-dimensional six-state clock model for the triangular lattice with periodic boundary conditions, as similarly reported in Refs. 13 and 14.

We begin by considering the experimental data obtained from as-grown $\mathrm{ErMnO_3}$ crystals. Figures 1(a) and 1(b) show two typical SEM images, illustrating the structural features of FE domains on the $a$-$b$ plane. It is recognizable in Fig. 1(a) that microstructure features in this area are apparently dominated by circular domains with amazing profiles. Furthermore, we also performed our extensive observations on the structures of domain walls, in particular for circlelike domains with sizes between 0.5 and 5 $\mu$m. Our observations demonstrate that, though certain single-wall domains can be observed, a large fraction of these annular domains in $\mathrm{ErMnO_3}$ adopt a double-wall structure as typically shown in the inserted image of Fig. 1(a), in which the two domain walls can be clearly seen as two bright circles. These facts suggest that the double-wall structure could be an energetically favored structural pattern in $\mathrm{ErMnO_3}$; certain similar domain walls have been also observed by Chae *et al.*[13].

In addition to the annular domains, extended stripe domains as generally discussed in conventional ferroelectric materials, such as $\mathrm{PbTiO_3}$,[15,16] also appear in the as-grown $\mathrm{ErMnO_3}$ crystals. Actually, we can often see notable domain bands caused evidently by the interplay among stripe and annular domains. In Fig. 1(b), we show a set of stripe domains and domain bands lining up roughly along the [110]-axis direction. It is notable that each domain band originates from a rectilinear ferroelectric domain which exhibits visible interaction with the annular domains; as a result, the stripe domains in Fig. 1(b) often adopt zigzag profiles surrounded by circular domains. Since stripe domain patterns are considered to be the ground state,[13] then the appearance of annular domains reveals that the system enters a low-energy excited state.

Another important issue of concern in the present study is the three-dimensional structural features of the annular domain structures. We therefore performed our observations perpendicular to the $c$-axis direction to reveal the side views of domain walls. Figures 1(c) and 1(d) show two examples of SEM and PFM images obtained for $\mathrm{ErMnO_3}$ crystals, respectively. It is recognizable that the side views of FE domains in $\mathrm{ErMnO_3}$ usually have elongated shapes along the

 

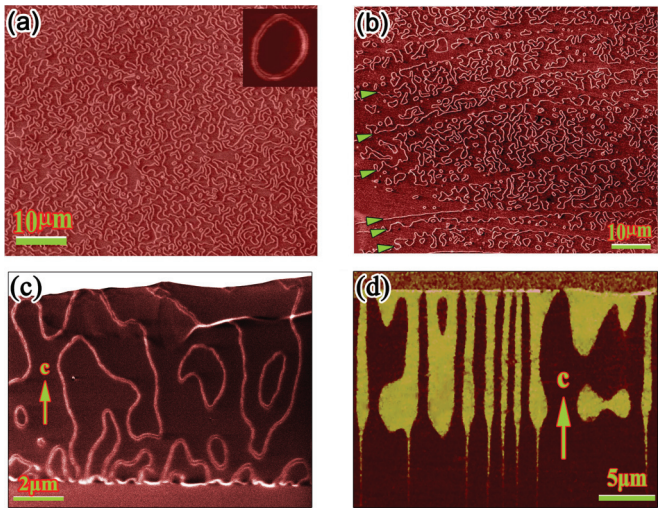


FIG. 1. (Color online) Structural features of ferroelectric domains in $ErMnO_3$. (a) SEM image of circular domains in the $a$-$b$ plane. The inset shows the double-wall structure. (b) SEM image showing the interaction of stripe domains (as indicated by arrows) with circular domains in the $a$-$b$ plane. (c) SEM and (d) PFM images showing the side views of circular FE domains in the $a$-$c$ plane. The annular structures can be recognized in certain areas.

$c$-axis direction due to the essential anisotropic properties of $R\mathrm{MnO_3}$ crystals. It is remarkable that certain domain walls are closed within the crystals yielding annular domains in the present system. A circle domain with one shell wall and an annular domain with double-shell walls can be clearly observed on this surface with some elongation along the $c$ axis. These results demonstrate that the energetically unfavorable charged domain walls can be protected not only by the vortex cores,[17] but also by annular structures. It is noted that the poling configuration of annular domains shows up very similar properties in comparison with the artificial structure, as illustrated in Ref. 18, which is considered to be potential electronic device elements used for spatial conductivity modulation. Careful analysis of experimental images taken along relevant orientations suggests that the FE domains in the present system frequently adopt annular structures composed of concentric shells. In Fig. 2, we show a series of structural models for FE circular domains with different shell structures [Fig. 2(a)] and the relevant experimental images of domain walls as observed by SEM [Fig. 2(b)]. It is recognizable that these circular structures can be well indexed, respectively, by their annular number $n$ (i.e., the domain shells). Importantly, it is also recognizable that FE onion domains with $n = 1$ show very similar structural features with the known magnetic bubble domains which have been used commonly to build electronic devices;[8,9] these facts suggest that these ferroelectric bubbles might be modulated by electric field.

In order to understand the essential structural features for the annular domains, we have employed the Monte Carlo simulations on the two-dimensional six-state clock model for the triangular lattice, and the Hamiltonian used in our study is similar to that in Refs. 13 and 14. The six distinctive states in the theoretical model correspond respectively to the known six domains, i.e., $\alpha^+$, $\beta^-$, $\gamma^+$, $\alpha^-$, $\beta^+$, and $\gamma^-$.[10] Figure 2(c) shows a typical result for structural domains within the KT

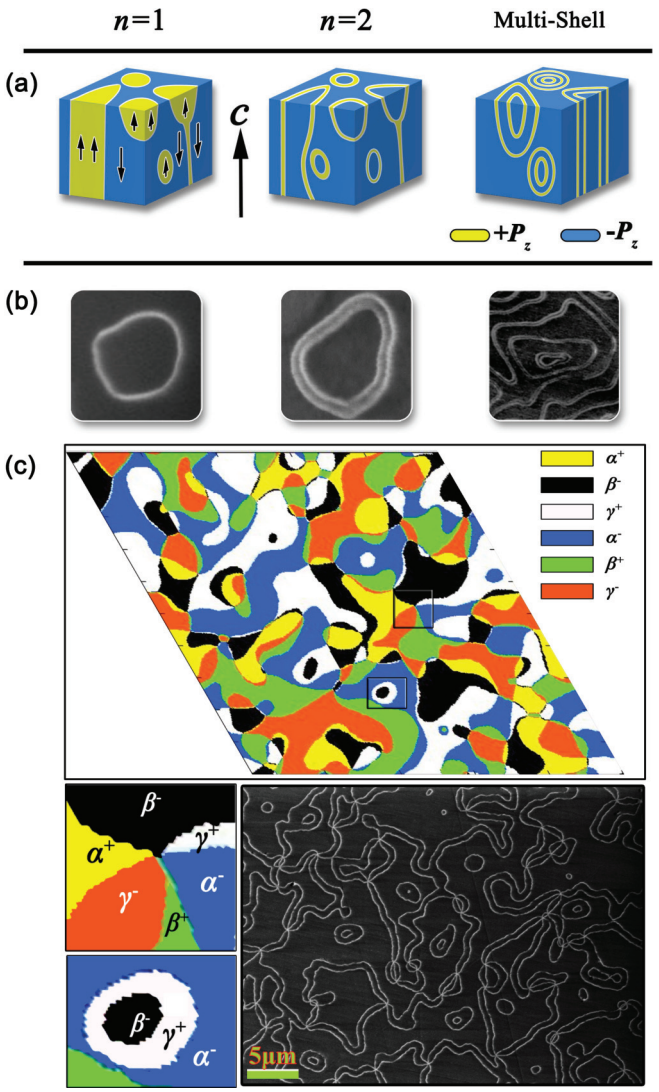


FIG. 2. (Color online) FE onion domains with shells of $n = 1, 2$, and multishell. (a) Structural models for FE onion domains observed in $R\mathrm{MnO_3}$. The $n = 1$ onion domain often shows poling features very similar to those of magnetic bubbles. Polarization in $R\mathrm{MnO_3}$ occurs along the $c$-axis direction as indicated by the arrows. (b) SEM images showing the domain walls for FE domains with different annular numbers in the $a$-$b$ plane. (c) The domain structures obtained from the six-state clock model in two dimensions through Monte Carlo simulations, showing the coexistence of cloverleaf vortices and annular domains. Lower panel: The left insets show the structural features and poling configurations for a vortex and an annular domain from the square marked areas. The right inset is an experimental image showing the coexistence of cloverleaf patterns and annular domains obtained from an annealed $ErMnO_3$ sample.

phase after 3500 Monte Carlo steps (MCS) per lattice at a temperature of $T = 0.1J/k$, where $J$ is the coupling constant and $k$ is the Boltzmann constant. It is visible that, in addition to vortex-antivortex pairs, the double-wall annular domains appear in many areas in the KT phase in good agreement with our experimental observations, as shown in the lower panel of Fig. 2(c). As the transition between long-range order and KT order is accompanied with a variation of correlation function and free energy, a large quantity of annular domains condense

while the vortex pairs are protected by their logarithmic entropy. However, a few residual annular domains still coexist with vortex pairs in the KT phase, so the so-called KT phase is a little different from the low-temperature phase in the $X$-$Y$ model in which only vortex-type topological excitations exist. This conclusion is demonstrated by our experimental and simulated results. The coexistence of circular-type and vortex-type excitations is also observed on the side surface parallel to the $c$ axis. It suggests a potential for experimental three-dimensional six-state clock model study. Moreover, the structural configurations, as well as the poling features, for each domain can be directly read out from this simulated image as clearly illustrated in the inset images. According to our theoretical data, the double-wall structure could have the configurations of $(\alpha^{+/-}\beta^{-/+}\gamma^{+/-})$ or $(\alpha^{+/-}\gamma^{-/+}\beta^{+/-})$. On the other hand, it is also noted that the annular domains could commonly appear at room temperature in $R\mathrm{MnO_3}$ crystals. This fact suggests that this kind of domain can also be arrested by slow kinetic and strong pinning features as discussed in Ref. 13.

We now consider the atomic structures in correlation with the poling configurations and mechanism for the formation of annular domains in $R\mathrm{MnO_3}$. Experimental investigations in the $R\mathrm{MnO_3}$ materials revealed that the FE domain structures can be evidently affected by the defect structures, especially the antiphase boundary. Previous study demonstrated that FE and antiphase domains in $R\mathrm{MnO_3}$ result essentially from the phase transition from $P6_3/mmc$ to a superstructure phase ($P6_3cm$); this superstructure phase adopts a $\sqrt{3}\times\sqrt{3}$ supercell and often contains three types of antiphase domains (so-called $\alpha$, $\beta$, and $\gamma$) and two types of antiphase boundaries as recognizable by relative phase shifts.[13,19] Actually, a clear view of the local polarization and antiphase boundaries (APB) can be directly obtained in the atomic resolution TEM images taken perpendicular to the $c$-axis direction. Figure 3(a) shows a typical aberration-corrected TEM image illustrating the alteration of poling direction crossing a FE domain wall (dotted line). In area A of the TEM image, the visible upward distortion for the two thirds of the Er ions in a trimerized pattern suggests an upward polarization in this area. On the other hand, the downward distortion of two thirds of Er ions in the area B demonstrates a reversed poling feature. In Fig. 3(b), we show a schematic illustration in the upper panel for the Er displacements as measured qualitatively for an Er layer as indicated by an arrow in Fig. 3(a). In order to facilitate the comparisons and structural analysis, we show three schematic pictures illustrating structural features of interlocked ferroelectric and antiphase boundaries in the lower panel of Fig. 3(b). It is exhibited that the ferroelectric boundaries can be interlocked respectively with two types of antiphase boundaries, i.e., (FEB + APB1) and (FEB + APB2). In comparison with the experimental data, we can conclude that the observed domain wall in Fig. 3(a) can be characterized as FEB + APB1. In Figs. 3(c) and 3(d), we show two simplified models for the concentric circular domains interlocked with the antiphase structures based on our experimental data, respectively. Figure 3(c) exhibits a structural model arising from a regular configuration of $\cdots\alpha^{+}\beta^{-}\gamma^{+}\alpha^{+}\beta^{-}\gamma^{+}\cdots$ for three types of antiphase domains. This model is in good agreement with the simulated data on the six-state clock model as illustrated in the above context. Figure 3(d) shows a possible

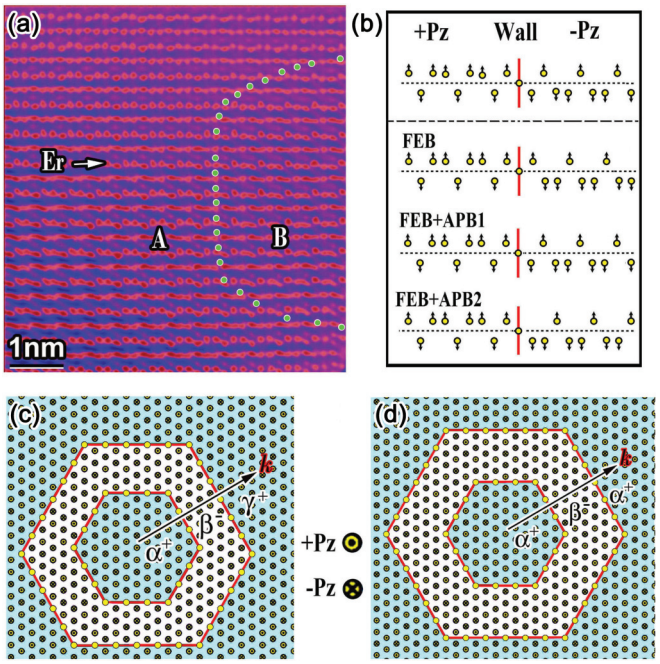


FIG. 3. (Color online) Atomic structure and interlocked FE domain walls in $\mathrm{ErMnO_3}$. (a) Cs-corrected TEM image shows the alteration of structural distortions crossing a domain wall as indicated by dotted line; this image is taken along the [110] direction with Cs = –13 $\mu$m, and Er and Mn atoms are shown as bright dots. (b) Upper panel: Structural distortions of Er ions crossing the wall as measured from the indicated Er layer in (a). Lower panel: Three schematic pictures for domain walls, FEB, FEB + APB1, and FEB + APB2. (c) Structural model for the annular domains arising from a periodic $\alpha^{+}\gamma^{-}\beta^{+}\ \alpha^{+}\gamma^{-}\beta^{+}\ \alpha^{+}\gamma^{-}\beta^{+}$ structure; the phase shifts at the boundaries are measured along the **k** direction. (d) A simplified structural model for the circular domains from a periodic $\alpha^{+}\beta^{-}\alpha^{+}\beta^{-}\alpha^{+}\beta^{-}$ structure.

structural model based on the alternative appearance of only two types of antiphase domains (i.e., $\alpha^{+}\beta^{-}\alpha^{+}\beta^{-}\alpha^{+}\beta^{-}$), which seldom appear in the simulations. It implies that this type of structure is unstable in this system and the two circle walls can be coalesced together and vanished.

In previous studies, structural changes of the vortex domains in $\mathrm{YMnO_3}$ have been studied under applied electric fields to reveal its dynamic features.[11] Based on our recent investigations, both the vortex and annular domains in $R\mathrm{MnO_3}$ could show visible dynamic phenomena depending on electron beam intensity during our SEM observations. Actually, we can see clear movements of domain walls and alternation of the domain configurations under an acceleration voltage of $V_0 = 1$ kV. Figures 4(a)–4(d) show four frames taken from a video of a crystal at different times. It is known that the average penetration depth of electron beam for $V_0 = 1$ kV is estimated to be 210 nm, which could result in visible charge redistribution and changes of poling properties.[12] On the other hand, the secondary electrons in SEM in general are emitted from a very thin surface layer (about 5–10 nm), so the experimental images just reveal changes of surface domain structures. Take an annular domain, for example: It has the double-layered walls as indicated by an arrow in Fig. 4(a); the polarization between these two walls can be determined to be along the

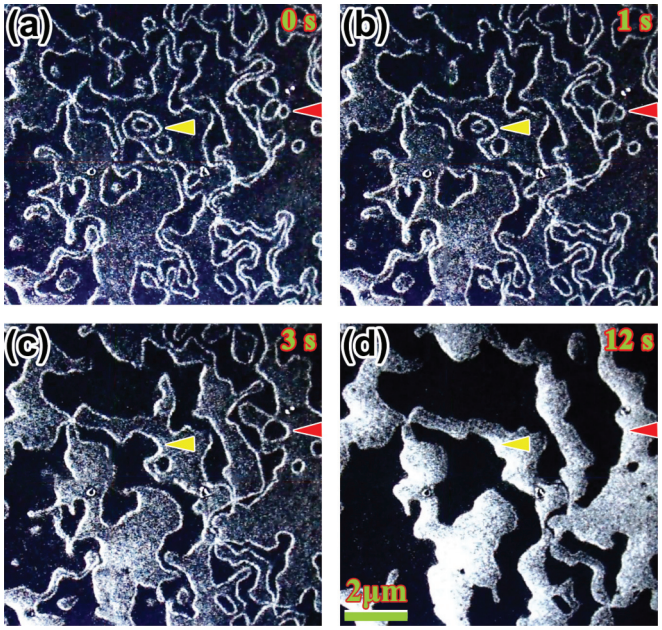


FIG. 4. (Color online) Dynamic features of annular domains in $R\mathrm{MnO_3}$ on the basic $a$-$b$ plane. (a)–(d) Four frames taken from a video reveal the motion of domain walls under electron irradiation. The evolution of an annular domain is indicated by a yellow arrow. The coalition between two single-layered domains is indicated by a red arrow.

view direction. Under electron irradiation, its outer wall tends to expand and, in contrast, the inner wall shrinks, and then the outer wall touches and coalesces with a nearby vortex as shown in Fig. 4(b). As a matter of fact, the radius of the inner circle could decrease continuously and, finally, totally disappears [see Fig. 4(c)]. Moreover, the coalition between two single-layered domains has been also noted on the right side of these images (indicated by red arrows). In the present case, it is noted that the domain reorganizations stop about 10 s later and yield remarkable large FE domains as shown in Fig. 4(b).

The interplay among domain walls can be also observed in our experiments. As mentioned in the above context, there are two kinds of domain walls; the experimental data clearly demonstrate that the boundary coalitions only happen among the same type of walls. In addition, according to our observations, two different kinds of walls never coalesce even they are close to each other. These facts suggest that the model shown in Fig. 3(c) is an energetically favored structure in the present system.

We now discuss the fundamental properties of multilayered annular domains in $R\mathrm{MnO_3}$. Figure 5(a) shows a SEM image displaying complex FE domain structures obtained in a $\mathrm{YMnO_3}$ crystal. The alternation of poling features from regular annuli at core area B to random vortices at areas A are clearly demonstrated by the PFM measurements shown in Fig. 5(b). In order to understand the evolutions of multilayered annular domains in correlation with the vortices, we performed a series of thermal annealing experiments, and the domain patterns checked in the crystals were cooled down from different temperatures to room temperature. Our observations show that the multilayered annular shells can be switched into the cloverleaf patterns just above the critical temperature $T_c$. As a

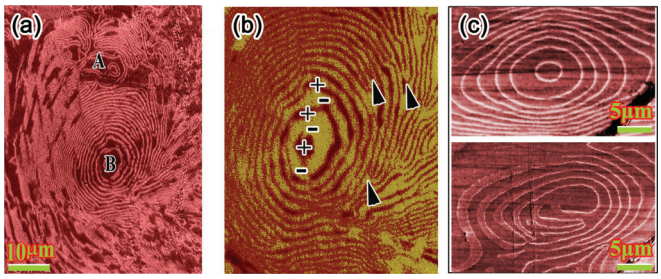


FIG. 5. (Color online) Ferroelectric annular domains in $R\mathrm{MnO_3}$ on the basic $a$-$b$ plane. (a) Annular pattern for a large onion domain in a $\mathrm{YMnO_3}$ crystal; the vortex patterns appear at the outer shells (area A). (b) PFM image showing the alternation of polarization in the annular domains of Fig. 5(a). The polarizations of the typical domains of $+P_z$ and $-P_z$ are illustrated by "+" and "–" respectively. (c) Thermal annealing effect on a large annular domain above the critical temperature $T_c$. The upper figure shows a SEM image of multilayered annular pattern in annealed $\mathrm{TmMnO_3}$ at 1170 °C which is nearly the same as observed in the as-grown sample. The lower one is obtained from the same area in the reannealed sample at 1250 °C.

result, certain large "vortex" and annular domains could also be observed in some areas. Figure 5(c) shows two SEM images of $\mathrm{TmMnO_3}$ single crystals clearly illustrating the thermal evolution and remarkable change of annular domain above the $T_c$. These crystals are observed after cooling it down quickly from 1170 °C and 1250 °C. Our observations demonstrate that the multilayered annular domains are rather stable below 1200 °C, and, on the other hand, they change evidently in samples annealed above about 1200 °C. It is important to point out that though the multilayered annular patterns with $n \geqq 3$ have not been found in our theoretical simulations, this multilayered annular domain structures have been widely observed in different samples such as $\mathrm{YMnO_3}$, $\mathrm{ErMnO_3}$, $\mathrm{TmMnO_3}$, $\mathrm{LuMnO_3}$, and $\mathrm{ScMnO_3}$. Though the formation and structural properties of multilayered domains have been investigated in a variety of samples based on our experimental observation, the mechanism for remarkable domains is still not clear. It is noted that the present structural defects or fissures (edges) in the crystals could evidently affect the annular domain structures.

In summary, our experimental observations and theoretical simulations for the FE domains demonstrate that annular domains can be stable in a large temperature range in the multiferroic $R\mathrm{MnO_3}$ materials, which appear in the KT phase coexisting with the cloverleaf vortices at high temperature and also being visible at room temperature associated with stripe domains. It is believed that the cloverleaf vortices and annular domains at low temperature are actually arrested by slow kinetic and strong pinning as discussed in Ref. 13. Based on *in situ* SEM observations, the dynamic features as well as the interaction of domain walls are analyzed. Moreover, the annular domains often show multilayered structures, and thermal annealing experiments directly show that the annular domains could change into cloverleaf vortices above the trimerization-structural transition temperature $T_c$. It is expected that the unique structural features of these domains could raise a series of new physical issues for further investigation, such as the poling and charging features on domain walls.

The authors thank J. Zhu for fruitful discussions and help with the TEM experiments. This work was supported by National Basic Research Program of China 973 Program (Grant Nos. 2011CBA00101, 2010CB923002, 2011CB921703, 2012CB821404), the Natural Science Foundation of China (Grant Nos. 11274368, 51272277, 11074292, 11004229, 11190022), the Special Fund of Tsinghua for basic research (Grant No. 201110810625) and Chinese Academy of Sciences. SWC was supported by NSF-DMR-1104484).

*Corresponding author: ljq@aphy.iphy.ac.cn

[1]J. F. Scott and C. A. Araujo, Science **246**, 1400 (1989).
[2]R. Waser and A. Rudiger, Nat. Mater. **3**, 81 (2004).
[3]C. H. Ahn, K. M. Rabe, and J. M. Triscoe, Science **303**, 488 (2004).
[4]Z. Q. Wu, N. D. Huang, Z. R. Liu, J. Wu, W. H. Duan, and B. L. Gu, J. Appl. Phys. **101**, 014112 (2007).
[5]K. Lee and S. Baik, Annu. Rev. Mater. Res. **36**, 81 (2006).
[6]H. W. Jang, D. Ortiz, S. H. Baek, C. M. Folkman, R. R. Das, P. Shafer, Y. B. Chen, C. T. Nelson, X. Q. Pan, R. Ramesh, and C. B. Eom, Adv. Mater. **21**, 817 (2009).
[7]G. S. Almasi, G. E. Keefe, and K. D. Teriep, AIP Conf. Proc. **10**, 207 (1972).
[8]T. H. O'Dell, *Magnetic Bubbles* (Macmillan, London, 1974).
[9]B. Cockayne, M. Chesswas, J. G. Plant, and A. W. Vere, J. Mater. Sci. **4**, 556 (1964).
[10]T. Choi, Y. Horibe, H. T. Yi, Y. J. Choi, W. Wu, and S. W. Cheong, Nat. Mater. **9**, 253 (2010).
[11]S. C. Chae, Y. Horibe, D. Y. Jeong, S. Rodan, N. Lee, and S. W. Cheong, Proc. Natl. Acad. Sci. USA **107**, 21366 (2010).
[12]J. Li, H. X. Yang, H. F. Tian, C. Ma, S. Zhang, Y. G. Zhao, and J. Q. Li, Appl. Phys. Lett. **100**, 152903 (2012).
[13]S. C. Chae, N. Lee, Y. Horibe, M. Tanimura, S. Mori, B. Gao, S. Carr, and S.-W. Cheong, Phys. Rev. Lett. **108**, 167603 (2012).
[14]G. S. Grest and D. J. Srolovitz, Phys. Rev. B **30**, 6535 (1984).
[15]S. K. Streiffer, J. A. Eastman, D. D. Fong, C. Thompson, A. Munkholm, M. V. Ramana Murty, O. Auciello, G. R. Bai, and G. B. Stephenson, Phys. Rev. Lett. **89**, 067601 (2002).
[16]D. D. Fong, G. B. Stephenson, S. K. Streiffer, J. A. Eastman, O. Auciello, P. H. Fuoss, and C. Thompson, Science **304**, 1650 (2004).
[17]D. Meier, J. Seidel, A. Cano, K. Delaney, Y. Kumagai, M. Mostovoy, N. A. Spaldin, R. Ramesh, and M. Fiebig, Nat. Mater. **11**, 284 (2012).
[18]R. K. Vasudevan, A. N. Morozovska, E. A. Eliseev, J. Britson, J.-C. Yang, Y.-H. Chu, P. Maksymovych, L. Q. Chen, V. Nagarajan, and S. V. Kalinin, Nano Lett. **12**, 5524 (2012).
[19]S. C. Abrahams, Acta Crystallogr. B **57**, 485 (2001).